ORIGINAL ARTICLE

Detrimental Effects of Diet-Induced Obesity on τ Pathology Are Independent of Insulin Resistance in τ Transgenic Mice

Antoine Leboucher,[1,2] Cyril Laurent,[1,2] Francisco-José Fernandez-Gomez,[1,2] Sylvie Burnouf,[1,2] Laetitia Troquier,[1,2] Sabiha Eddarkaoui,[1,2] Dominique Demeyer,[1,2] Raphaëlle Caillierez,[1,2] Nadège Zommer,[1,2] Emmanuelle Vallez,[1,3,4] Kadiombo Bantubungi,[1,3,4] Christophe Breton,[1,5] Pascal Pigny,[1,2,6] Valérie Buée-Scherrer,[1,2] Bart Staels,[1,3,4] Malika Hamdane,[1,2] Anne Tailleux,[1,3,4] Luc Buée,[1,2,6] and David Blum[1,2,6]

The τ pathology found in Alzheimer disease (AD) is crucial in cognitive decline. Midlife development of obesity, a major risk factor of insulin resistance and type 2 diabetes, increases the risk of dementia and AD later in life. The impact of obesity on AD risk has been suggested to be related to central insulin resistance, secondary to peripheral insulin resistance. The effects of diet-induced obesity (DIO) on τ pathology remain unknown. In this study, we evaluated effects of a high-fat diet, given at an early pathological stage, in the THY-Tau22 transgenic mouse model of progressive AD-like τ pathology. We found that early and progressive obesity potentiated spatial learning deficits as well as hippocampal τ pathology at a later stage. Surprisingly, THY-Tau22 mice did not exhibit peripheral insulin resistance. Further, pathological worsening occurred while hippocampal insulin signaling was upregulated. Together, our data demonstrate that DIO worsens τ phosphorylation and learning abilities in τ transgenic mice independently from peripheral/central insulin resistance.
***Diabetes* 62:1681–1688, 2013**

Accumulation and aggregation of hyperphosphorylated τ proteins (τ pathology) into neurofibrillary tangles (NFT) is a major pathological process encountered in Alzheimer disease (AD) (1). NFT are observed early in life and increase during ageing in hippocampal area (2). In AD, the spatiotemporal progression of NFT from the hippocampus to isocortical areas correlates to cognitive deficits (3), supporting an instrumental role of τ pathology in memory deficits.

Individual components of the metabolic syndrome have been linked to the risk of developing cognitive impairments and AD (for reviews, see Refs. 4 and 5). Particularly, midlife development of obesity, a risk factor for insulin resistance and type 2 diabetes, was described to increase the risk of dementia and AD later in life (6,7). Also,

morbidly obese elderly individuals exhibit enhanced hippocampal τ phosphorylation (8). The detrimental effect of obesity on τ phosphorylation observed in the brain of AD patients might arise from central insulin resistance, which develops secondary to peripheral resistance (9–11). In line, central disruption of insulin signaling by insulin receptor or insulin receptor substrate (IRS) 2 gene deletion or following intracerebral streptozotocine injections leads to τ hyperphosphorylation (12–15). However, none of these studies have been performed in models developing an AD-like τ pathology. Moreover, the effects of early and progressive development of diet-induced obesity (DIO) upon τ pathology and associated memory deficits remain unknown. In this study, we evaluated the effects of high-fat diet (HFD) feeding, at an early pathological stage, on later pathophysiological development in THY-Tau22 transgenic mice, a model developing progressive hippocampal τ pathology and spatial memory defects (16). Our data demonstrate that DIO worsens τ phosphorylation and learning abilities in τ transgenic mice independently from peripheral/central insulin resistance.

RESEARCH DESIGN AND METHODS

Animals and diets. THY-Tau22 male mice (C57BL6/J background) were generated by overexpression of human four-repeat τ mutated at sites G272 V and P301S under the control of Thy1.2 promoter (16). Nontransgenic littermates (wild-type [WT]) were used as controls. A total of 42 mice of each genotype were housed three per cage as previously described (17). All protocols were approved by an ethical committee (AF 06/2010, Comité d'éthique en expérimentation animale Nord-pas-de-Calais [CEEA]). THY-Tau22 mice (T) and WT littermates (W) were fed with chow (C) diet (RM1A; Special Diets Services, Essex, U.K.) or HFD (H; 59% kcal from fat; D12331; Ssniff). A total of 42 animals of each genotype were assigned to balanced groups (WT chow [WC], WT HFD [WH], τ chow [TC], and τ HFD [TH]; $n = 21$/group) according to their initial body weight (WC, 22.4 ± 0.4; WH, 22.3 ± 0.3; TC, 20.4 ± 0.2; and TH, 20.4 ± 0.3 g), glycemia (WC, 150.5 ± 6.0; WH, 148.0 ± 5.2; TC, 156.0 ± 4.6; and TH, 154.3 ± 4.6 mg/dL), and insulinemia (WC, 0.31 ± 0.03; WH, 0.29 ± 0.04; TC, 0.28 ± 0.03; and TH, 0.30 ± 0.05 μg/L). Body weights were measured weekly. Noteworthy, body weights of THY-Tau22 mice at the onset of the experiment (i.e., 2-month-old mice) were significantly lower compared with WT littermates ($P < 0.001$, using Student t test).

Plasma parameters. Plasma was collected at baseline and following 20 weeks of treatment at the tail vein after a 6-h fasting, and parameters were determined as follows: blood glucose (Accu-Chek Performa glucometer; Roche Diagnostics GmbH); plasma insulin and leptin measured, respectively, using ultrasensitive insulin ELISA (Mercodia AB), and mouse/rat leptin enzyme immunoassay kit (Sipbio). Total and HDL-cholesterol as well as triglycerides were measured by enzymatic method using ready-to-use kits (Biomérieux). Non–HDL-cholesterol levels were calculated by substracting HDL from total cholesterol.

Glucose and insulin tolerance tests. Both intraperitoneal glucose tolerance test and insulin tolerance tests were performed following a 6-h fast. D(+) glucose (1 g/kg; Sigma-Aldrich) or insulin (0.75 units/kg in saline; Actrapid

See accompanying commentary, p. 1365.

Penfill; Novo Nordisk) were injected intraperitoneally. Blood glucose was then measured at 0, 15, 30, 60, 90, and 120 min following injection.

Spatial learning assessment using the Morris water maze. A 100-cm circular pool was filled with opacified water and kept at 21°C as previously described (18). A 10-cm round platform was hidden 1 cm beneath the surface of the water at a fixed position. Each mouse was given four swimming trials per day (20 min intertrial interval) for 4 consecutive days. The start position was pseudorandomized across trials. Time required to locate the hidden escape platform (escape latency) and distance traveled (path length) were recorded using the Ethovision XT tracking system (Noldus).

Sacrifice. At completion of the experiment (i.e., following 20 weeks of diet), mice were about 7 months old and killed after 6 h fasting by cervical dislocation, and brains were removed. Brains from five mice per group were postfixed for 7 days in 4% paraformaldehyde and then incubated in 20% sucrose for 24 h and kept frozen at −80°C until use. Hippocampi of the remaining animals were dissected out using a coronal acrylic slicer (Deltamicroscopies) at 4°C and stored at −80°C until use. Remaining samples were homogenized in 200 μL Tris buffer (pH 7.4) containing 10% sucrose and protease inhibitors (Complete; Roche Diagnostics GmbH), sonicated, and kept at −80°C for biochemical experiments.

Immunohistochemistry. Serial free-floating sagittal sections (40 μm) were obtained using a cryostat (Leica Microsystems GmbH). Immunohistochemistry was performed as previously described (17) using antibodies raised against phosphorylated (AT8; pSer202/205; Pierce) and abnormally phosphorylated (AP422; pSer422; BioSource International) τ species. 3,3′-Diaminobenzidine pixel count was performed blindly on six hippocampal sections per animal separated by 280 μm by setting the threshold to the same value for each section as previously described (17) using ImageJ software (Scion Software).

Biochemical analysis. Total protein extracts were obtained and analyzed as previously described (18). Bidimensional electrophoresis experiments were performed as previously described (18). Briefly, lysates were precipitated with methanol/chloroform. A total of 15 μg of proteins was dissolved in two-dimensional buffer (7 mol/L urea, 2 mol/L thiourea, 4% 3-[(3-cholamidopropyl) dimethylammonio]-1-propanesulfonate, and 0.6% pharmalytes). Lysates were loaded on immobilized pH gradient strip 3–11 ReadyStrip (Amersham GE) and isoelectrofocused with the Protean IEF cell (Amersham GE) according to the manufacturer's instructions. The strips were layered onto a 4–12% Bis-Tris polyacrylamide gel. Membranes were incubated with total τ antibody (Cter).

For Sarkosyl-soluble/insoluble protein preparations, hippocampi were homogenized by sonication in a lysis buffer containing 10 mmol/L Tris-HCl (pH 7.4), 0.32 mol/L sucrose, 800 mmol/L NaCl, and 1 mmol/L EGTA with protease inhibitors (Complete w/o EDTA; Roche) and centrifuged at 12,000*g* for 10 min at 4°C. The supernatant incubated 1 h in 1% Sarkosyl (*N*-lauroylsarcosine sodium salt; Sigma-Aldrich) at room temperature was then centrifuged at 100,000*g* for 1 h at 4°C, thus forming the supernatant and pellet containing Sarkosyl-soluble and -insoluble τ species, respectively. Sarkosyl-insoluble proteins were directly resuspended in lithium dodecyl sulfate (LDS) 2×, and sarkosyl-soluble samples were mixed with LDS 2× supplemented with reducing agents (Invitrogen). Sarkosyl-soluble and Sarkosyl-insoluble samples were loaded onto NuPAGE Novex gels (Invitrogen) with a ratio of 1:12.

For Western blots, protein amounts were evaluated using the BCA assay (Pierce), subsequently diluted with LDS 2× supplemented with reducing agents (Invitrogen), and then separated on NuPAGE Novex gels (Invitrogen). Proteins were transferred to nitrocellulose membranes, which were then saturated (5% nonfat dry milk or 5% BSA) in Tris 15 mmol/L (pH 8), NaCl 140 mmol/L, and 0.05% Tween and incubated with primary and secondary antibodies. Signals were visualized using chemiluminescence kits (ECL; Amersham Bioscience) and a LAS3000 imaging system (Fujifilm). Results were normalized to β-actin, and quantifications were performed using ImageJ software (Scion Software). Total proteins were quantified versus β-actin. Phosphorylated proteins were quantified versus total counterpart.

τ Antibodies included anti–phospho(p)-Thr181 (AT270), pThr212/pSer214 (AT100), pThr231 (AT180) (Pierce); pThr202/pSer205 (AT8; Thermo Scientific); pS262, pSer396, pSer404, pSer422 (Invitrogen); Tau1 (recognizing dephosphorylated τ; Millipore); and total τ Cter (homemade antibody recognizing the 11 amino acids in COOH-terminal part of τ). Antibodies directed against neuronal markers included anti-NeuN, synaptophysin, spinophilin (Millipore); and neuron-specific enolase (Enzo LifeScience). Antibodies targeting kinases and related proteins included anti-Akt, pSer473-Akt, Ca2+/calmodulin-dependent protein kinase II (CaMKII), pThr286-CaMKII, Erk1/2 (p42/44 mitogen-activated protein kinase [MAPK]), pThr202/Tyr204-Erk1/2, pSer9–glycogen synthase kinase 3β (GSK3β), p38 MAPK, pThr180/pTyr182-p38 MAPK, pSer16-Pin1, protein kinase A (PKA), pThr197-PKA, stress-activated protein kinase/JNK, pThr183/pTyr185–stress-activated protein kinase/JNK (Cell Signaling Technology); anti-CDK5, GSK3α/β, p25-p35; anti-pTyr216–GSK3β, PP2A-C catalytic (Millipore); and anti-pTyr307–PP2A-C (Abcam). Antibodies directed against insulin-signaling actors included anti–insulin receptor β, IRS1, pSer612-IRS1, IRS2, phosphatidylinositol 3-kinase (PI3K)/P85, pThr458-PI3K/P85 (Cell Signaling Technology); and PTP1B (Abcam). β-Actin antibody was from Sigma-Aldrich.

Protein phosphatase assay. Phosphatase activity measurements were performed using the molybdate-based colorimetric Serine/Threonine Phosphatase Assay System (Promega), according to the manufacturer's instructions.

Statistics. Results are expressed as means ± SEM. Differences between mean values were determined using the Student *t* test, two-way ANOVA (2W-ANOVA), or one-way ANOVA (1W-ANOVA) followed by a post hoc Fisher least significant difference test using GraphPad Prism Software (GraphPad). The P values <0.05 were considered significant.

RESULTS

HFD induces obesity but not insulin resistance in THY-Tau22 mice. THY-Tau22 ($n = 21$/group) and WT ($n = 21$/group) mice were fed chow or HFD, starting at an age when τ pathology and memory impairments are slight or even absent in THY-Tau22 mice (2 months) until ~7 months of age, when pathology is significant (Supplementary Fig. 1). Although a significant lower body weight was observed between TC mice and WC mice ($P < 0.037$, using 2W-ANOVA), HFD-fed WT and THY-Tau22 animals progressively and similarly developed obesity, reaching, respectively, 182 ± 5 and 174 ± 5% of the initial body weight, at completion of the experiment (WH vs. WC and TH vs. TC, $P < 0.001$; WH vs. TH, $P = 0.94$ using 2W-ANOVA; Fig. 1*A*). WH and TH mice exhibited significant and similar increases in circulating leptin (Supplementary Fig. 2), white adipose tissue mass (Supplementary Fig. 2), as well as plasma triglycerides, cholesterol, HDL-cholesterol, and non–HDL-cholesterol concentrations (Supplementary Fig. 2). HFD feeding led to a significant increase in fasting glycemia and insulinemia in WT and THY-Tau22 mice. However, although both plasma glucose and insulin were similar between WC and TC animals (Fig. 1*B* and *C*), they were significantly lower in TH as compared with WH mice (glucose: WH, 239 ± 8 vs. TH, 207 ± 5 mg/dL, $P < 0.001$; insulin: WH, 1.8 ± 0.2 vs. TH, 1.4 ± 0.2 μg/L, $P < 0.05$ using 1W-ANOVA). In accordance, the homeostasis model assessment of insulin resistance was significantly lower in TH versus WH mice (15.1 ± 1.4 vs. 23.5 ± 2.2; $P < 0.01$). WC and TC mice exhibited similar glucose tolerance ($P = 0.44$; Fig. 1*D* and *E*) and response to insulin ($P = 0.15$; Fig. 1*F* and *G*). Glucose tolerance was markedly and similarly impaired by the HFD ($P < 0.001$ vs. respective chow groups; WH vs. TH, $P = 0.11$ using 2W-ANOVA; Fig. 1*D* and *E*). However, surprisingly, although WH mice exhibited a significant attenuation of glucose lowering after insulin injection as compared with WC animals ($P < 0.001$), TH mice did not ($P = 0.20$ vs. TC; $P = 0.004$ vs. WH using 2W-ANOVA; Fig. 1*F* and *G*), suggesting that, unlike WH animals, TH mice do not develop peripheral insulin resistance.

HFD worsens spatial learning in THY-Tau22 mice. TC mice exhibited increased escape latency and path length as compared with WC animals (Fig. 2*A* and *B*; $P = 0.0013$ and $P = 0.03$, respectively, using 2W-ANOVA). Although the HFD did not exert any significant influence on these parameters in WT animals ($P = 0.96$ and $P = 0.36$), it further increased both parameters in TH mice (TC vs. TH, escape latency, $P = 0.037$, and path length, $P = 0.027$, using 2W-ANOVA). Consistently, spatial learning was significantly different between WH and TH animals ($P < 0.001$ and $P = 0.0012$). Day-by-day analysis demonstrates that chow-fed THY-Tau22 mice performed significantly worse that WT animals at days 3 and 4 ($P < 0.05$) and indicate that, as compared with chow-fed THY-Tau22 mice,
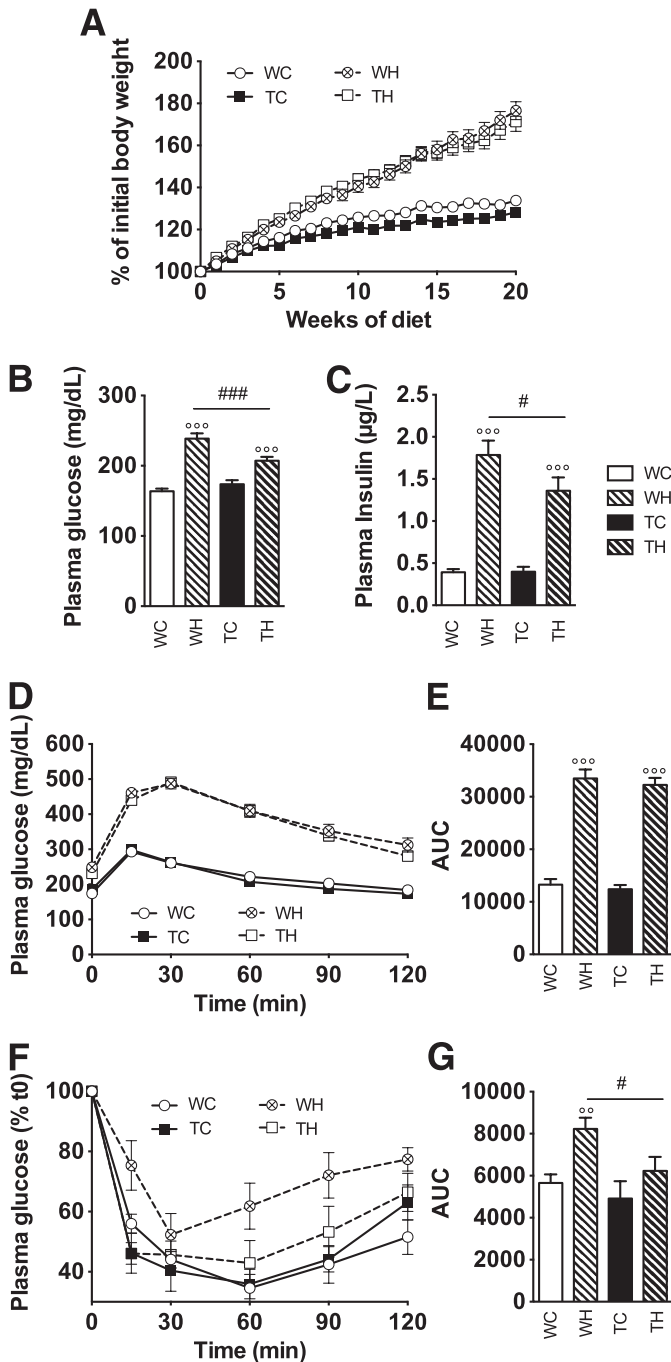
FIG. 1. HFD leads to obesity in absence of insulin resistance in THY-Tau22 mice. *A*: Progressive establishment of a diet-induced obesity in WT and THY-Tau22 mice (WC vs. WH, $P < 0.001$; TC vs. TH, $P < 0.001$, using 2W-ANOVA). *B* and *C*: Glucose (*B*) and insulin (*C*) levels at completion of experiment. *D* and *E*: Intraperitoneal glucose tolerance test demonstrated significant and similar impairments in HFD-fed mice regardless of genotype (WC vs. WH and TC vs. TH, $P < 0.001$ using 2W-ANOVA). *F* and *G*: Insulin tolerance test demonstrated significant attenuation of glucose lowering following insulin injection in WH mice as compared with WC animals ($P < 0.001$ using 2W-ANOVA). Conversely, TH mice were not significantly different from TC animals ($P = 0.20$ vs. TC group using 2W-ANOVA). *E* and *G* represent areas under the curve (AUC) calculated from data presented in *F* and *H*, respectively. Results are expressed as means ± SEM. °°$P < 0.01$, °°°$P < 0.001$ vs. respective chow; #$P < 0.05$, ###$P < 0.001$ vs. TH mice using 1W-ANOVA. Open circles/open bars, WC; black squares/black bars, TC; crossed circles/dashed bars, WH; open squares/black dashed bars, TH.

performances of HFD-fed THY-Tau22 mice were lower at days 1 and 2 ($P < 0.05$).

Velocity did not differ between groups ($P > 0.05$, not shown). Worsening of spatial learning in TC mice was not associated with major structural hippocampal changes since neither CA1 thickness (not shown) nor expressions of neuronal (NeuN and neuron-specific enolase) and synaptic markers (Spinophilin; Supplementary Fig. 3) were changed.

HFD feeding potentiates τ phosphorylation in THY-Tau22 mice. Given the important number of phosphorylation sites on τ (>80) (1), we first performed a two-dimensional electrophoresis analysis and observed a significant shift of human τ isovariants from the basic to the acidic pH range in the TH group as compared with TC mice (arrow, Fig. 3*A*) consistent with an increased phosphorylation. Evaluation of several τ phosphoepitopes using SDS-PAGE (Fig. 3*B*) showed that the HFD did not induce a global increase in τ phosphorylation. Rather, it promoted increased phosphorylation on specific τ phosphoepitopes. Thus, although phosphorylation at Thr181, Ser212/Thr214 (AT100), Thr231, Ser262, and Ser396 remained unchanged (Fig. 3*B*), phosphorylation at Ser214 and Ser404 as well as abnormal phosphorylation at Ser422 were found significantly increased by HFD, respectively, reaching 182 ± 35, 167 ± 17, and 151 ± 17% of TC mice ($P = 0.037$, $P = 0.0028$, and $P = 0.018$ vs. TC using Student t test). Immunohistochemical hippocampal analysis confirmed these changes. Phosphorylation was significantly increased in TH versus TC animals at both pSer202/Thr205 (AT8) and pSer422
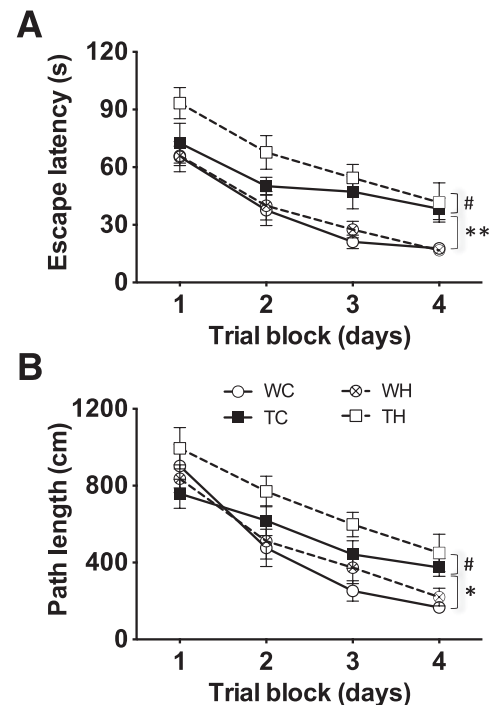

FIG. 2. HFD potentiates spatial learning impairments in THY-Tau22 mice. TC animals exhibited significantly increased escape latency (*A*) and path length (*B*) as compared with WC animals. Although HFD did not exert significant influence on both parameters in WT animals, escape latency and path length were further increased in TH mice as compared with TC animals. Results are expressed as means ± SEM. WC vs. TC: *$P < 0.05$, **$P < 0.01$; TC vs. TH: #$P < 0.05$ using 2W-ANOVA. Open circles, WC; black squares, TC; crossed circles, WH; open squares, TH.
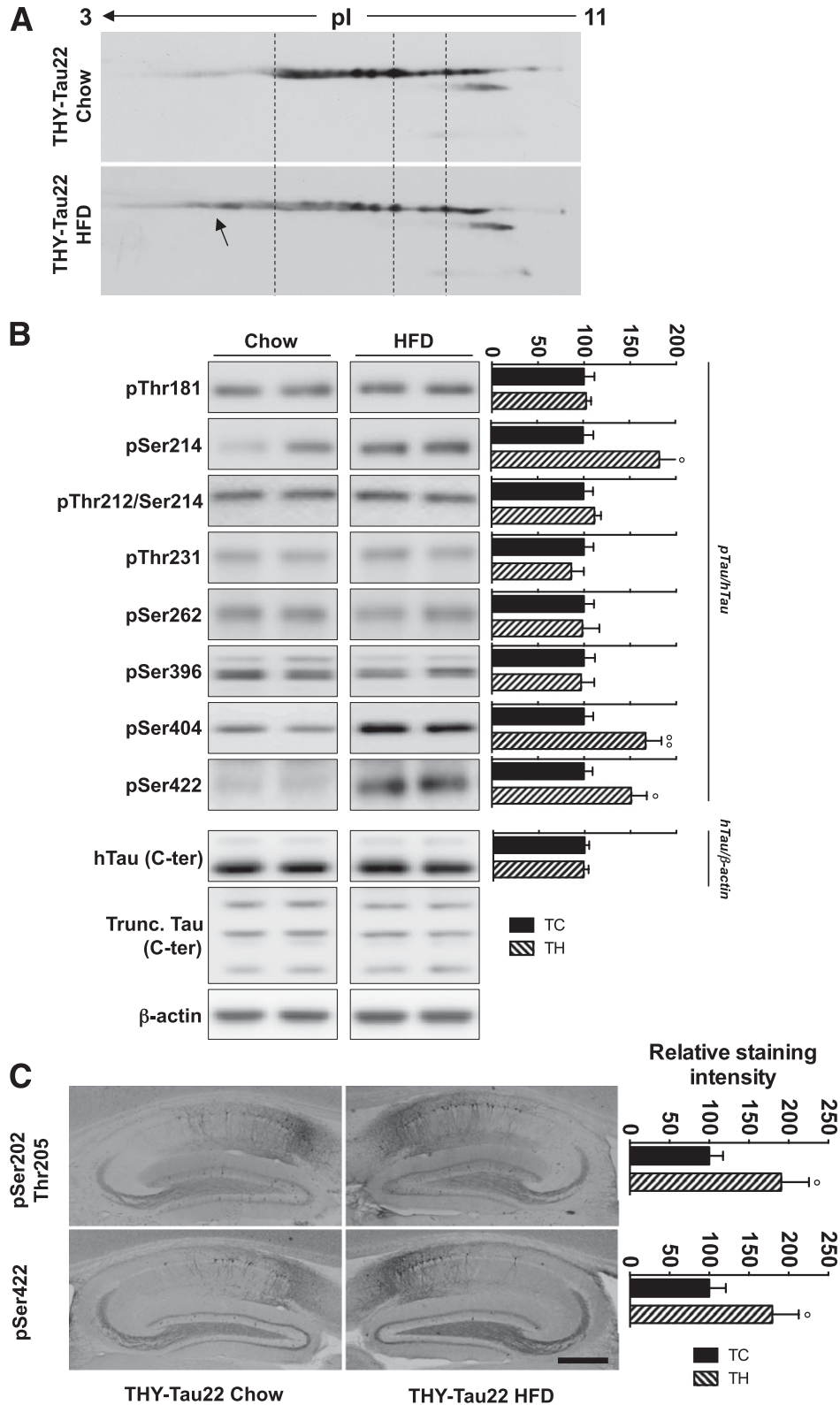
FIG. 3. HFD increases hippocampal τ phosphorylation in THY-Tau22 mice. *A*: Representative two-dimensional profile of total human τ (hTau) in TC (*top*) and TH (*bottom*) animals showing an increase in τ acidic species in the TH animals (arrow). *B*: SDS-PAGE analysis of τ phosphorylation in TC and TH animals using antibodies targeting physiological (pThr181, pSer214, pThr231, pSer262, pSer396, and pSer404) and pathological (pThr212/Ser214 and pSer422) epitopes. As shown in the *left* panel, significant enhancement of τ phosphorylation at Ser214, Ser404, and Ser422 was observed in TH mice. This occurred in absence of change in total hTau expression or τ proteolysis (Trunc. Tau). Quantifications of phosphoepitopes were performed vs. total hTau. hTau quantification was performed vs. β-actin. Results are expressed as percentage of TC animals. *C*: Immunohistochemical analyses of hippocampal τ phosphorylation at pSer202/Thr205 (*top left*) and pSer422 (*bottom left*). Scale bar, 500 μm. Results are expressed as means ± SEM. °$P < 0.05$, °°$P < 0.01$ vs. TC using Student t test ($n = 5–7$/group). Black bars, TC; black dashed bars, TH. pI, isoelectric point.

epitopes (respectively, 190 ± 35% of TC, P = 0.021, and 179 ± 33% of TC, P = 0.039, using Student t test; Fig. 3C). Expression of total human τ and of its proteolytic fragments was not modified by HFD (Fig. 3B). To study the impact of the HFD on τ aggregation, biochemical fractionation was performed, and Sarkosyl-soluble and -insoluble fractions were analyzed. The amount of Sarkosyl-insoluble τ remained similar in chow and HFD-fed THY-Tau22 mice (Supplementary Fig. 4). Conversely to THY-Tau22 animals, HFD-fed WT animals did not exhibit changes in endogenous murine τ phosphorylation as shown by two-dimensional electrophoresis and evaluation of several murine τ phosphoepitopes (Supplementary Fig. 5). However, the total level of murine τ was significantly increased in WH mice versus WC animals (Supplementary Fig. 5).

Effects of HFD feeding on hippocampal kinases and phosphatases. τ Phosphorylation is under the tight control of kinase/phosphatase activities. More than 30 different kinases are able to phosphorylate τ (1). Therefore, we assessed the effects of HFD on major τ kinases (Akt, GSK3β, CaMKII, ERK1/2, cdk5, p38, JNK, and PKA). HFD feeding did not alter total expression levels of the studied kinases in the hippocampus of THY-Tau22 mice (Fig. 4 and Supplementary Fig. 6). The p35/p25 ratio, representative of deregulated cdk5 activity, was unchanged in TH mice (Supplementary Fig. 6). Phosphorylation at the Tyr216 epitope of GSK3β remained unaltered in TH animals, whereas a significant increase of phosphorylation at its inactivating Ser9 epitope was observed (136 ± 15% of TC, P = 0.05; Fig. 4A). HFD feeding also led to a significant increase of Ser473-Akt and Thr286-CaMKII phosphorylation in THY-Tau22 mice, reaching, respectively, 165 ± 16 (P = 0.006) and 171 ± 23% (P = 0.028) of chow-fed THY-Tau22 animals (Fig. 4A). Finally, phosphatase activity was not significantly changed in the hippocampus of TH animals (TC: 94 ± 23 vs. TH: 119 ± 8 pmol phosphate/h/µg protein; P = 0.34, Student t test; n = 4/group; not shown). Accordingly, expression and phosphorylation of the catalytic subunit of PP2A, the main τ phosphatase, remained unchanged in TH mice (Supplementary Fig. 6). In line with the absence of global phosphorylation changes on τ, the HFD did not modify phosphorylation/expression of neither Akt, GSK3β, and CaMKII (Supplementary Fig. 7) nor ERK, p38-MAPK, JNK, and PP2A-C (not shown) in WT animals.

HFD feeding upregulates hippocampal insulin signaling in THY-Tau22 mice. Increased τ phosphorylation was previously observed in experimental conditions mimicking brain insulin resistance (12–15). Strikingly, our data support that insulin signaling rather increases in the hippocampus of TH animals. Indeed, besides increased phosphorylation of Akt at Ser473 and GSK3β at Ser9 (Fig. 4A), increased expression of IRS1 (55 ± 12% vs. TC; P = 0.0076, Student t test) as well as a trend toward decreased phosphorylation at its inhibitory Ser612 epitope (−24 ± 7% of TC, P = 0.09; Fig. 4B) were observed. This was associated with a slightly increased phosphorylation of the p85 subunit of PI3K at Thr458 (33 ± 12% of TC, P = 0.08 using Student t test; Fig. 4B). Conversely, HFD feeding of WT animals did not influence hippocampal insulin signaling (Supplementary Fig. 7).

DISCUSSION

In a transgenic model of progressive AD-like τ pathology, our results demonstrate for the first time that early life DIO worsens both spatial memory and τ phosphorylation later in life in a manner independent from insulin resistance.

DIO potentiated τ hyperphosphorylation and spatial memory impairments in THY-Tau22 mice. Further, although HFD feeding did not potentiate τ aggregation, significant phosphorylation changes at specific physiological (pSer202/Thr205, pSer214, and pSer404) and pathological (pSer422) epitopes in THY-Tau22 mice were induced. Given the important number of phosphorylation sites on τ (>80) (1), others are also likely to be modified by the HFD in THY-Tau22 mice, as suggested by the increase in τ phosphorylation seen using two-dimensional electrophoresis. τ hyperphosphorylation has been consistently associated with cognitive alterations in several dementing disorders (19) and τ transgenic models (20,21) and also associated with impaired spatial memory in WT animals treated with 3,4-methylenedioxymethamphetamine or sevoflurane in the absence of any τ aggregation (18,22). This supports that memory worsening is likely due to τ hyperphosphorylation at specific phosphoepitopes. This is also in line with previous findings showing, in regulatable τ transgenic animals developing τ hyperphosphorylation, that memory impairments occur dissociated from τ aggregation (23).

τ Phosphorylation is under the control of phosphatases, essentially PP2A, and a number of distinct kinases (>30) (1). Increased τ phosphorylation thus likely resulted from a disrupted kinase/phosphatase balance in TH mice. Our data rule out changes at the phosphatase level. Rather, we observed elevated activation of Akt and CaMKII in HFD-fed versus chow-fed THY-Tau22 mice. Previous studies suggested that τ phosphorylation at Ser214 can be mediated by Akt (24–26) and that the latter is associated with the spatiotemporal sequence of AT8 (pSer202/Thr205) immunoreactivity and NFT in AD brains (27). Phosphorylation of Akt, and of its Ser9-GSK3β target, was also previously observed in mice undergoing repeated anesthesia, exhibiting persistent τ phosphorylation and cognitive deficits (18). Increased CaMKII activity could contribute to τ hyperphosphorylation on the Ser214, Ser404, Ser422, and Ser202/Thr205 epitopes through direct interaction or following sequential processes (28–30). Noteworthy, in contrast to THY-Tau22 mice, HFD-fed WT animals exhibited neither an increase in endogenous murine τ phosphorylation nor a change at the kinase level. Rather, a significant increase in total murine τ levels was observed. Interestingly, this occurs in HFD-fed WT mice that exhibit peripheral insulin resistance and no activation of hippocampal insulin signaling. Although the functional significance of these observations remain unclear, since HFD-fed WT animals did not exhibit memory defects, they are in accordance with previous data showing that peripheral and/or central insulin resistance increases endogenous τ expression (10,15).

Peripheral insulin resistance is able to promote central insulin resistance (9–11) and is believed to trigger or, at least, contribute to key pathophysiological events underlying AD (31,32), including τ phosphorylation (12–14). Surprisingly, our data indicate that, in contrast to WT animals, HFD-fed THY-Tau22 mice do not develop peripheral insulin resistance. THY-Tau22 mice thus exhibit metabolic perturbations. Although the mechanisms underlying such differences between THY-Tau22 mice and WT littermates are currently unclear, human τ expression is not detected in peripheral organs (liver, pancreas, muscle, and adipose tissue; not shown), suggesting a central instead of peripheral effect.
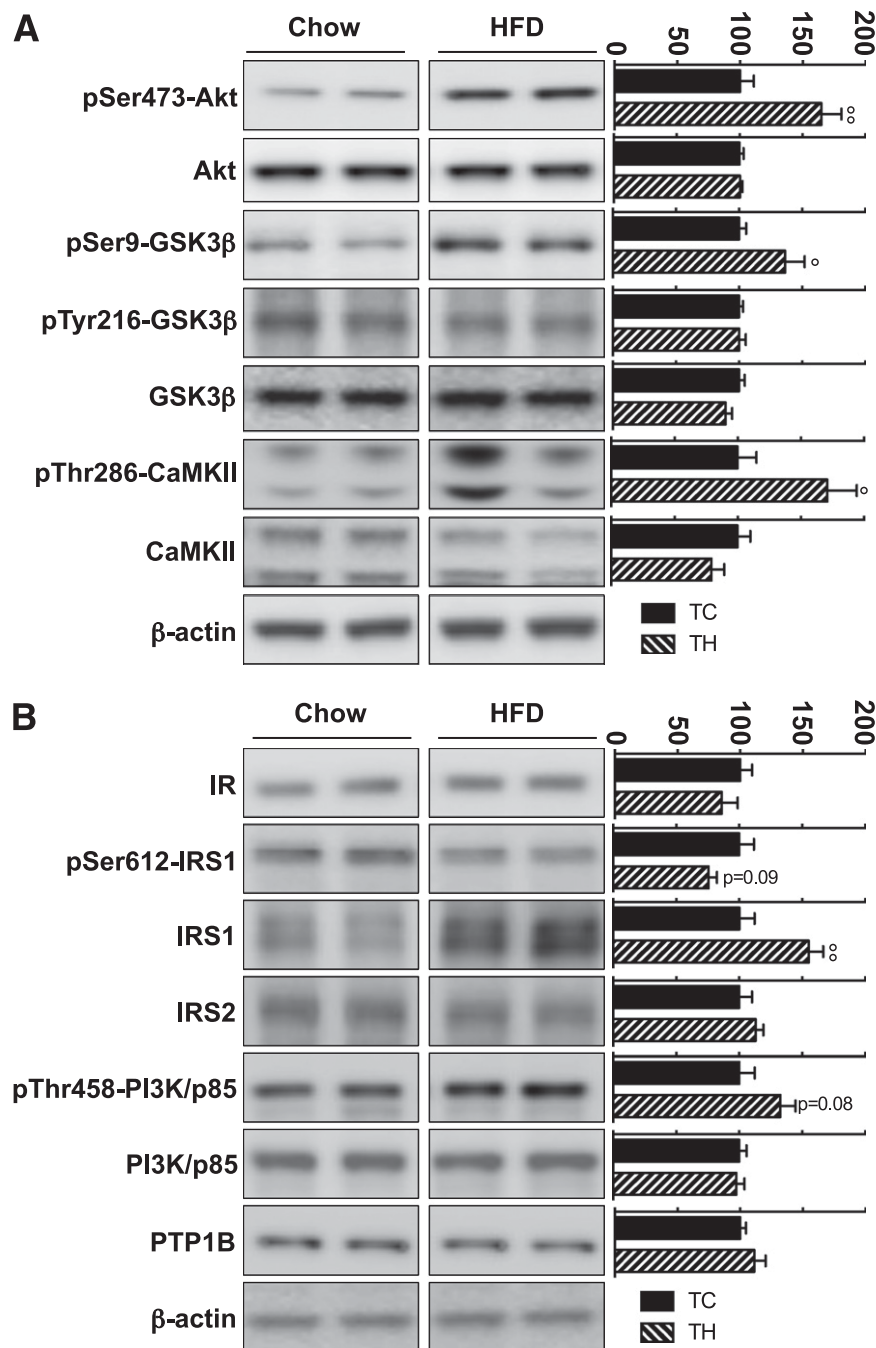
FIG. 4. Impact of HFD feeding on hippocampal τ kinases and insulin signaling in THY-Tau22 mice. SDS-PAGE analysis was performed using antibodies raised against total and phosphorylated forms of several τ kinases (*A*) or several components of insulin signaling (*B*). Results indicate a significant activation of Akt and CaMKII in TH animals together with an upregulation of insulin signaling. Phosphoepitopes were quantified vs. total form of respective protein. Total expressions were quantified vs. β-actin. Results are expressed as means percentage ± SEM of TC animals. °$P < 0.05$, °°$P < 0.01$ vs. TC animals, using Student *t* test ($n = 6$ to 7/group). Black bars, TC; black dashed bars, TH. IR, insulin receptor.

The relationships between central insulin signaling and τ phosphorylation in DIO models have yielded conflicting results in WT animals (10,33,34). Interestingly, our data indicate that hippocampal insulin signaling is upregulated in TH mice, attested by increased phosphorylation of Akt at Ser473, GSK3β at Ser9, and PI3K-p85 at Thr458, effects not observed in HFD-fed WT animals, which develop peripheral insulin resistance, as well as increased IRS1 expression and activity, exemplified by reduced inactivating phosphorylation of IRS1 at Ser612. Previous reports associated central insulin resistance, promoted by either

deletion of the insulin receptor and its IRS2 adaptor or intracerebral streptozotocine injections (12–14), with τ hyperphosphorylation. However, although mimicking impaired insulin signaling found in AD brains (31,32), none of these genetic or pharmacological models promote homogeneous patterns of τ hyperphosphorylation and kinase/phosphatase imbalance (12–14,35). Finally, none of them reproduce τ hyperphosphorylation and kinase profiles observed in TH mice. Given that THY-Tau22 mice did not exhibit brain insulin resistance, worsening of AD-like τ pathology induced by DIO may thus involve other obesity-associated

factors, the nature of which remain unknown. One contributing factor could be the dyslipidemia. Indeed, previous reports indicate that cholesterol-rich diets increase τ phosphorylation at the Ser202/Thr205 epitopes in τ transgenic animals (see Ref. 36 and discussion in this study). In addition, cholesterol-lowering compounds have been shown to be protective in τ transgenic mice (37).

In conclusion, our data show that early development of obesity increases τ burden and associated memory alterations later in life in a τ transgenic model. Such worsening appears dissociated from peripheral insulin resistance and associated with hippocampal upregulation of insulin signaling.

REFERENCES

1. Sergeant N, Bretteville A, Hamdane M, et al. Biochemistry of Tau in Alzheimer's disease and related neurological disorders. Expert Rev Proteomics 2008;5:207–224
2. Braak H, Thal DR, Ghebremedhin E, Del Tredici K. Stages of the pathologic process in Alzheimer disease: age categories from 1 to 100 years. J Neuropathol Exp Neurol 2011;70:960–969
3. Grober E, Dickson D, Sliwinski MJ, et al. Memory and mental status correlates of modified Braak staging. Neurobiol Aging 1999;20:573–579
4. Frisardi V, Solfrizzi V, Seripa D, et al. Metabolic-cognitive syndrome: a cross-talk between metabolic syndrome and Alzheimer's disease. Ageing Res Rev 2010;9:399–417
5. Pasinetti GM, Eberstein JA. Metabolic syndrome and the role of dietary lifestyles in Alzheimer's disease. J Neurochem 2008;106:1503–1514
6. Whitmer RA, Gustafson DR, Barrett-Connor E, Haan MN, Gunderson EP, Yaffe K. Central obesity and increased risk of dementia more than three decades later. Neurology 2008;71:1057–1064
7. Kivipelto M, Ngandu T, Fratiglioni L, et al. Obesity and vascular risk factors at midlife and the risk of dementia and Alzheimer disease. Arch Neurol 2005;62:1556–1560
8. Mrak RE. Alzheimer-type neuropathological changes in morbidly obese elderly individuals. Clin Neuropathol 2009;28:40–45
9. Mielke JG, Taghibiglou C, Liu L, et al. A biochemical and functional characterization of diet-induced brain insulin resistance. J Neurochem 2005;93:1568–1578
10. Moroz N, Tong M, Longato L, Xu H, de la Monte SM. Limited Alzheimer-type neurodegeneration in experimental obesity and type 2 diabetes mellitus. J Alzheimers Dis 2008;15:29–44
11. Pratchayasakul W, Kerdphoo S, Petsophonsakul P, Pongchaidecha A, Chattipakorn N, Chattipakorn SC. Effects of high-fat diet on insulin receptor function in rat hippocampus and the level of neuronal corticosterone. Life Sci 2011;88:619–627
12. Schubert M, Brazil DP, Burks DJ, et al. Insulin receptor substrate-2 deficiency impairs brain growth and promotes tau phosphorylation. J Neurosci 2003;23:7084–7092
13. Schubert M, Gautam D, Surjo D, et al. Role for neuronal insulin resistance in neurodegenerative diseases. Proc Natl Acad Sci USA 2004;101:3100–3105
14. Deng Y, Li B, Liu Y, Iqbal K, Grundke-Iqbal I, Gong C-X. Dysregulation of insulin signaling, glucose transporters, O-GlcNAcylation, and phosphorylation of tau and neurofilaments in the brain: Implication for Alzheimer's disease. Am J Pathol 2009;175:2089–2098
15. Grünblatt E, Salkovic-Petrisic M, Osmanovic J, Riederer P, Hoyer S. Brain insulin system dysfunction in streptozotocin intracerebroventricularly treated rats generates hyperphosphorylated tau protein. J Neurochem 2007;101:757–770
16. Schindowski K, Bretteville A, Leroy K, et al. Alzheimer's disease-like tau neuropathology leads to memory deficits and loss of functional synapses in a novel mutated tau transgenic mouse without any motor deficits. Am J Pathol 2006;169:599–616
17. Belarbi K, Burnouf S, Fernandez-Gomez F-J, et al. Beneficial effects of exercise in a transgenic mouse model of Alzheimer's disease-like Tau pathology. Neurobiol Dis 2011;43:486–494
18. Le Freche H, Brouillette J, Fernandez-Gomez F-J, et al. Tau phosphorylation and sevoflurane anesthesia: an association to postoperative cognitive impairment. Anesthesiology 2012;116:779–787
19. Bierer LM, Hof PR, Purohit DP, et al. Neocortical neurofibrillary tangles correlate with dementia severity in Alzheimer's disease. Arch Neurol 1995;52:81–88
20. Rosenmann H, Grigoriadis N, Eldar-Levy H, et al. A novel transgenic mouse expressing double mutant tau driven by its natural promoter exhibits tauopathy characteristics. Exp Neurol 2008;212:71–84
21. Van der Jeugd A, Ahmed T, Burnouf S, et al. Hippocampal tauopathy in tau transgenic mice coincides with impaired hippocampus-dependent learning and memory, and attenuated late-phase long-term depression of synaptic transmission. Neurobiol Learn Mem 2011;95:296–304
22. Busceti CL, Biagioni F, Riozzi B, et al. Enhanced tau phosphorylation in the hippocampus of mice treated with 3,4-methylenedioxymethamphetamine ("Ecstasy"). J Neurosci 2008;28:3234–3245
23. Santacruz K, Lewis J, Spires T, et al. Tau suppression in a neurodegenerative mouse model improves memory function. Science 2005;309:476–481
24. Kyoung Pyo H, Lovati E, Pasinetti GM, Ksiezak-Reding H. Phosphorylation of tau at THR212 and SER214 in human neuronal and glial cultures: the role of AKT. Neuroscience 2004;127:649–658
25. Griffin RJ, Moloney A, Kelliher M, et al. Activation of Akt/PKB, increased phosphorylation of Akt substrates and loss and altered distribution of Akt and PTEN are features of Alzheimer's disease pathology. J Neurochem 2005;93:105–117
26. Ksiezak-Reding H, Pyo HK, Feinstein B, Pasinetti GM. Akt/PKB kinase phosphorylates separately Thr212 and Ser214 of tau protein in vitro. Biochim Biophys Acta 2003;1639:159–168
27. Pei J-J, Khatoon S, An W-L, et al. Role of protein kinase B in Alzheimer's neurofibrillary pathology. Acta Neuropathol 2003;105:381–392
28. Yoshimura Y, Ichinose T, Yamauchi T. Phosphorylation of tau protein to sites found in Alzheimer's disease brain is catalyzed by Ca2+/calmodulin-dependent protein kinase II as demonstrated tandem mass spectrometry. Neurosci Lett 2003;353:185–188
29. Singh TJ, Grundke-Iqbal I, Wu WQ, et al. Protein kinase C and calcium/calmodulin-dependent protein kinase II phosphorylate three-repeat and

four-repeat tau isoforms at different rates. Mol Cell Biochem 1997;168:141–148

30. Wang J-Z, Grundke-Iqbal I, Iqbal K. Kinases and phosphatases and tau sites involved in Alzheimer neurofibrillary degeneration. Eur J Neurosci 2007;25:59–68

31. Talbot K, Wang H-Y, Kazi H, et al. Demonstrated brain insulin resistance in Alzheimer's disease patients is associated with IGF-1 resistance, IRS-1 dysregulation, and cognitive decline. J Clin Invest 2012;122:1316–1338

32. de la Monte SM. Brain insulin resistance and deficiency as therapeutic targets in Alzheimer's disease. Curr Alzheimer Res 2012;9:35–66

33. Becker K, Freude S, Zemva J, Stöhr O, Krone W, Schubert M. Chronic peripheral hyperinsulinemia has no substantial influence on tau phosphorylation in vivo. Neurosci Lett 2012;516:306–310

34. Jeon BT, Jeong EA, Shin HJ, et al. Resveratrol attenuates obesity-associated peripheral and central inflammation and improves memory deficit in mice fed a high-fat diet. Diabetes 2012;61:1444–1454

35. Killick R, Scales G, Leroy K, et al. Deletion of Irs2 reduces amyloid deposition and rescues behavioural deficits in APP transgenic mice. Biochem Biophys Res Commun 2009;386:257–262

36. Glöckner F, Meske V, Lütjohann D, Ohm TG. Dietary cholesterol and its effect on tau protein: a study in apolipoprotein E-deficient and P301L human tau mice. J Neuropathol Exp Neurol 2011;70:292–301

37. Boimel M, Grigoriadis N, Lourbopoulos A, et al. Statins reduce the neurofibrillary tangle burden in a mouse model of tauopathy. J Neuropathol Exp Neurol 2009;68:314–325